Discrete element modelling of geocell–reinforced track ballast under static and cyclic loading

Y. Liu[1], A. Deng[2] and M.B. Jaksa[3]

[1]School of Civil, Environmental and Mining Engineering, the University of Adelaide, SA 5005; PH (+61 8) 8313 0591; FAX: (+61 8) 8313 4359; email: yang.liu@adelaide.edu.au
[2]School of Civil, Environmental and Mining Engineering, the University of Adelaide, SA 5005; PH (+61 8) 8313 2830; FAX: (+61 8) 8313 4359; email: an.deng@adelaide.edu.au
[3]School of Civil, Environmental and Mining Engineering, the University of Adelaide, SA 5005; PH (+61 8) 8313 5135; FAX: (+61 8) 8313 4359; email: mark.jaksa@adelaide.edu.au

ABSTRACT

A geocell is a geosynthetic material developed to reinforce soils and aggregates. Similar to the configuration of a honeycomb, a geocell panel is designed to encompass consecutive confined cells where soils and aggregates are placed. The cellular confinement system of the geocell is beneficial in the reinforcement of track ballast, which helps restrain lateral movement and minimise vertical subsidence of a trackbed. To gain an understanding of the reinforcement, a numerical study has been conducted. The study uses the discrete element method to simulate the interaction between the geocell and the discrete particles of ballast. Both static and cyclic loading environments are considered. Displacements and stresses at both micro- and macro-scales are assessed for control and reinforced scenarios. The outcomes of this study seek to encourage likely reduction in trackbed thickness and width, to save construction cost and improve the sustainability of the railway trackbed.

Keywords: DEM, PFC, railway, ballast, geocell

1. INTRODUCTION

Rail transport is one of the major means of conveyance of passengers and goods worldwide. Due to the cyclic impact of trains, breakage and rearrangement occurs to the ballast in the trackbed of a railway. As a result, the trackbed is prone to lateral creep and subsidence, which is deemed to undermine the serviceability of rail tracks, and likely cause catastrophic failure of the tracks. To gauge the serviceability of the tracks, a significant amount of expense is spent annually to maintain the serviceability of rail tracks. To minimise this expense, a variety of engineered methods has been suggested and attempted to reinforce the ballast of the trackbed, such as embedment of geosynthetics (Indraratna *et al*. 2010, Chen *et al*. 2012) into the regime of ballast. Of these geosynthetics options, geocells are an emerging and promising means of reinforcing railway ballast.

Geocells are a cellular confinement system created by the U.S. Army Corps of Engineers to reinforce cohesionless soils. Through developments and applications over the past decades, geocells have been deployed in a variety of infrastructure situations such as foundations, slopes and retaining structures. Both experimental and numerical studies, such as Yang (2010), and Dash (2012), have shown that geocell embedment improves performance of the infrastructure by reinforcing granular infill materials. More recently, a study by Leshchinsky and Ling (2013) was conducted to use geocell to reinforce railway ballast. The study employed the finite element (FE) method to model the mechanical response of the geocell–reinforced ballast. The FE method, however, is not an ideal tool in regard to representing ballast in that the ballast is comprised of discrete aggregate which violates the condition of continuum media when applying the FE method. In addition, most commercially-available FE software packages incorporate constitutive models valid for fine-grained soils and sands, which are generally unsuitable to model accurately the stress–strain behaviour of ballast. In contrast, an alternative numerical method is employed to model the mechanical response of geocell–reinforced ballast.

The discrete element method (DEM) possesses the capability to replicate, within engineering accuracy, distinct ballast aggregates, and to simulate the motion of the aggregate. Not only are the particles modelled by discrete geometric assemblages, but the mechanical parameters, such as stiffness and friction of the aggregate, are also calibrated against laboratory test results describing the major

stress–strain relationship of the aggregate. More importantly, 3D modelling can be achieved, which involves replicating a volume of ballast in the form of a trackbed embankment. Subjected to geocell reinforcement and various loading conditions, the 3D modelling is able to predict the mechanical response of the trackbed at both the macro- and micro-scales and the prediction offers a complete assessment in regard to the performance of the ballast trackbed. In this context, this study adopts the commercial DEM software package, *PFC3D* (ITASCA 2008), to simulate the geocell-reinforced ballast trackbed subjected to both static and cyclic loading. A control model is also established to evaluate the effectiveness of introducing a geocell into the trackbed.

2. DISCRETE ELEMENT MODELLING

2.1 Simulations of geocell

As *PFC3D* is able only to consider modelling spheres, the geocell is simulated by bonding individual spheres into a continuous medium, as shown in Figure 1. The spheres have a diameter of 5 mm, which is equivalent to the thickness of a real cell wall. Each cell is configured to honour the dimensions of the actual cell: 75 mm depth and 175 mm × 175 mm in side width. A total of 8 cells are generated and combined to form a section of geocell panel, being 742 mm × 495 mm from edge-to-edge. The short side (495 mm) aligns with the transverse plane of the trackbed and represents the dimensions of a geocell panel used in practice. Given the geometry of the geocell panel, the entire panel is composed of 12,762 parallel bonded spheres.

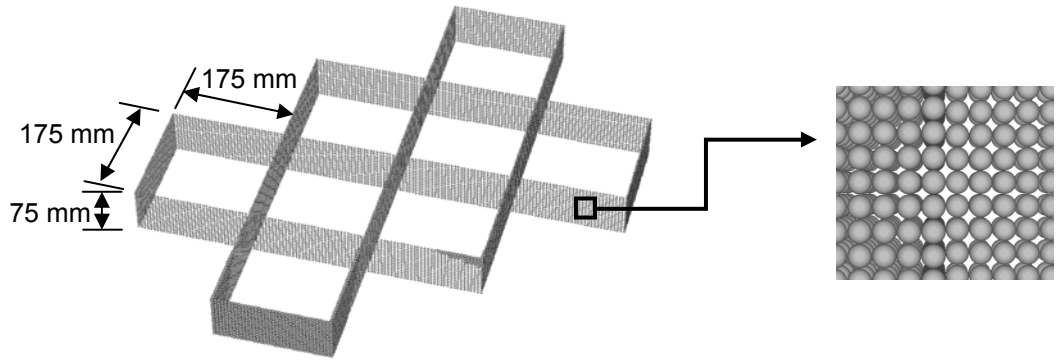

Figure 1. Simulation of geocell panel

The adopted input parameters for the spheres and their parallel bonds are shown in Table 1. Some of the parameters are obtained from the material supplier, such as density and friction coefficient. The remainder were evaluated from calibrations conducted against laboratory tensile strength tests, as well as from the relationship proposed by Potyondy and Cundall (2004). The displacement–stress calibration is summarised in Figure 2. As the parallel bond is not designed to model plastic deformation, there is a disparity between the simulation and test results. Nevertheless, the numerical simulation reproduces the peak tensile strength of the geocell specimen and reflects an appropriate trend of the displacement–stress relationship.

Table 1: Parameters for spheres used to simulate geocell

Parameter	**Value**
Parallel bond normal stiffness (N/m)	2.8×10^7
Parallel bond shear stiffness (N/m)	4.5×10^6
Parallel bond normal strength (N)	6.8×10^7
Parallel bond shear strength (N)	6.5×10^7
Parallel bond radius (mm)	2.5
Normal contact bond strength (N)	2.4×10^3
Shear contact bond strength (N)	2.4×10^3
Normal stiffness (N/m)	3.2×10^3
Shear stiffness (N/m)	3.2×10^3
Density (kg/m^3)	950
Frictional coefficient	0.5

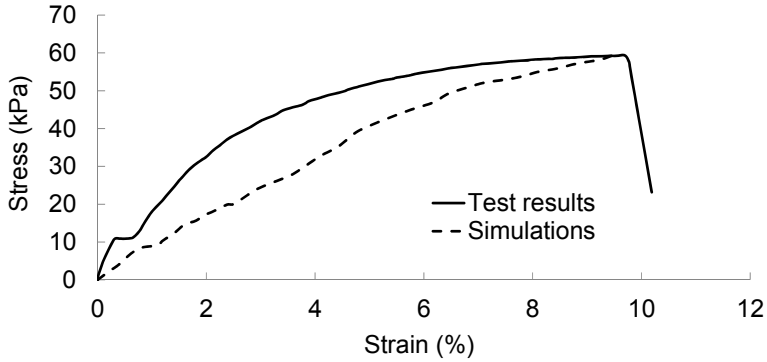

Figure 2. Tensile strength of geocell specimen

2.2 Simulations of ballast

Trackbed ballast is usually obtained by blasting and fragmenting a rock mass. Therefore, ballast is generally angular and irregular. To model effectively this angularity, the ballast is simulated as a clump of spheres, instead of a single sphere. Such a clump-based replication has been attempted recently, such as by Le Pen *et al*. (2013), which has shown that it outperforms spherical-based simulations. On account of the major shapes and angularity of ballast, 4 clump templates are developed to represent the general geometric configuration of ballast: trapozoidal, triangular, rectangular, and hexagonal. The shapes and sphere numbers for each clump are summarised in Table 2. In this study, the bonding force within a clump was set high enough to avoid particle fracture under normal loading conditions.

Table 2: Clump templates developed to simulate ballast

Shape of clump	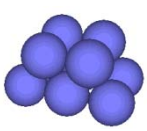	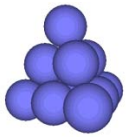	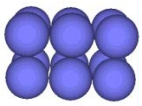	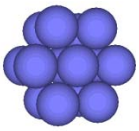
	Trapozoidal	Triangular	Rectangular	Hexagonal
Number of spheres for one clump	10	10	12	14

Similar to the method adopted to determine the input parameters for the geocell, stress–strain relationships under triaxial compression test conditions were used to calibrate the parameters for the ballast. Test data presented by Indraratna *et al*. (1998) were used in this calibration. A cylindrical mould of similar size to that of the test data (300 mm diameter x 600 mm height), was established using *PFC3D*. The mould was initially loaded with a number of spheres of varying diameters, 20 mm to 50 mm, as shown in Figure 3(a). The diameter was determined in accordance with the grading characteristics of the ballast presented by Indraratna *et al*. (1998). The spheres were then replaced, at equal volume, with the clump templates shown in Table 2. The replacement was conducted in equal allocations between the 4 templates. *PFC3D* assigned the templates to the existing spheres automatically so that the clumps were distributed within the mould randomly. The process of assigning clump templates, however, caused non-negligible inter-clump contact forces which are incompatible with subsequent loading scenarios. To negate these forces, the method developed by Lu and McDowell (2006) was employed. The wall of the mould was allowed to move outward at an extremely slow rate of 0.1 mm/time step until an equilibrium of zero contact force was achieved, as shown in Figure 3(b). Then, gravity was applied to the individual clumps. The final porosity of the volume of clumps in the mould was 0.39. A total of 632 clumps (7,584 spheres), were used to generate the triaxial compression test specimen.

Specimens were subjected to standard triaxial compression tests. A series of confining pressures were examined: 15, 30, 60, 90, 120 and 240 kPa, which are consistent with the pressures adopted by the data presented by Indraratna *et al*. (1998). The axial loading rate was set at 0.045 mm/s. This rate is low enough to capture the appropriate stress-strain relationship of each specimen. The loading was continued until an axial strain of 20% was reached. The servo-control mechanism (Itasca 2008) was applied to ensure the confining pressure the specimen was subjected to remained constant throughout the loading phase.

An iterative approach was adopted to determine the input parameters for the geocell. Figure 4 shows the simulated results compared with the test data presented by Indraratna *et al*. (1998) in terms of deviator stress vs. axial strain and volumetric strain vs. axial strain. The adopted input parameters used for the simulations are summarised in Table 3. As can be seen from Figure 4, very good agreement is obtained, which confirms the input parameters are validated with respect to simulating ballast aggregates using sphere clumps. These parameters are used for both static and cyclic loading cases.

2.3 Simulations of railway trackbed and loading

The railway trackbed was simulated in accordance with design guidelines published by the Australian Rail Track Corporation (ARTC) (2011). Figure 5(a) shows the geometry of the simulated 3D trackbed embankment, 480 mm wide at the crest, 930 mm wide at the base, 150 mm high and 1,000 mm long.

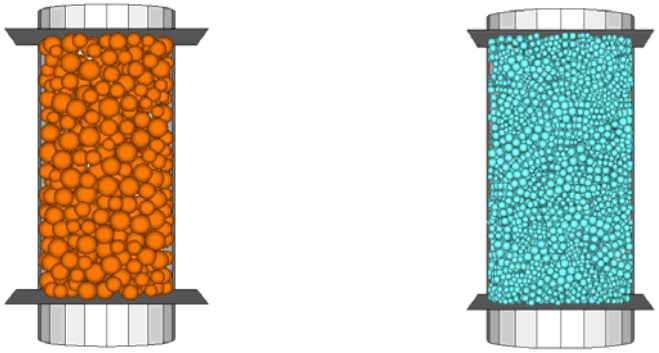

Figure 3. Ballast simulated by clumps in a triaxial test specimen: (a) assembly before, and (b) assembly after replacing spheres with clump templates

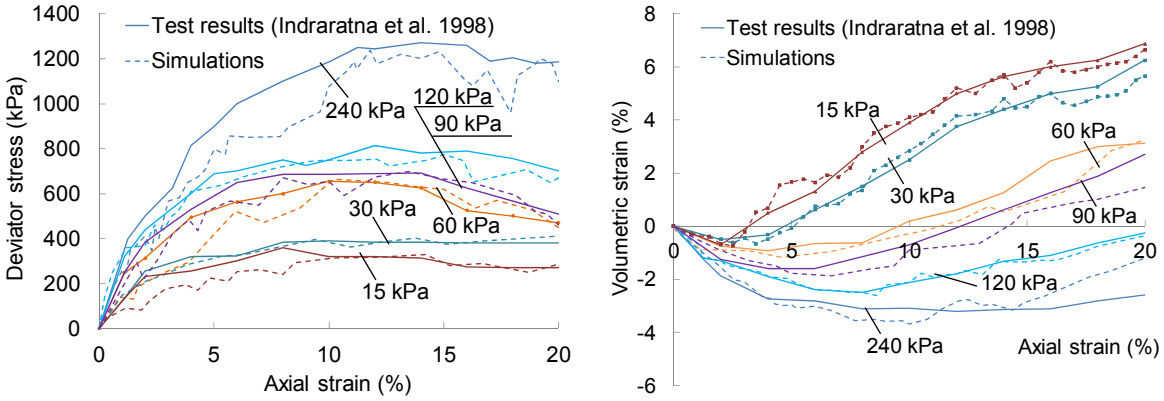

Figure 4. Triaxial results: (a) deviator stress vs. axial strain, and (b) volumetric strain vs. axial strain

Table 3: Parameters for clumps used to simulate ballast

Parameters	**Value**
Parallel bond normal stiffness (N/m)	1.8×10^5
Parallel bond shear stiffness (N/m)	1.8×10^5
Parallel bond normal strength (N)	6×10^{10}
Parallel bond shear strength (N)	6×10^{10}
Frictional coefficient	1
Density (kg/m^3)	2,500
Normal stiffness (N/m)	5×10^9
Shear stiffness (N/m)	1×10^9
Clump size (mm)	20 – 50

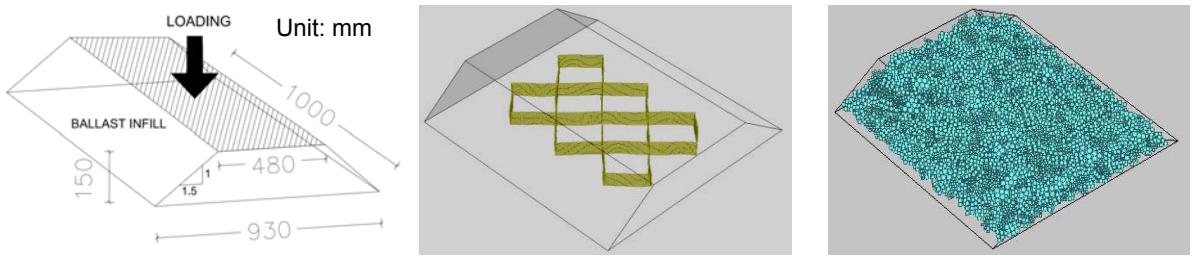

(a) (b) (c)

Figure 5. Simulation of railway trackbed: (a) geometric model, (b) in-place geocell, and (c) geocell-reinforced ballast trackbed

The base of the embankment is wider than the short side of the geocell panel configured in preceding part (495 mm). This is so that both margins at the base are free from the geocell reinforcement which optimises material usage. In longitudinal direction, the length of 1,000 mm is sufficient in relation to the long side (742 mm) of the geocell panel. On account of the two-dimensional nature of the trackbed (i.e. no longitudinal ballast movement), the front and rear cross-sectional planes are simulated with fixed walls, respectively. The normal stiffness and shear stiffness of both walls are 1×10^{10} N/m, which is much higher than those of the clumps. In order to reflect trackbed subsidence caused by the underlying subgrade, the subgrade is represented by a 'soft' wall that has lower stiffness (1×10^{8} N/m for normal and shear stiffness) than the ballast clumps.

Figures 5(b) and (c) shows the simulations of the geocell reinforcement and ballast infill. Both are generated using the same circumstances as those for calibration purposes. Regarding the ballast infill, temporary walls were used on the slope and upper surfaces of the trackbed to confine the clumps. To negate the inter-clump contact forces, the temporary walls were allowed to move outwards slightly and slowly. Once the clumps were established, with no preloaded forces, the temporary walls were removed. A surcharge pressure of 1 kPa was applied to the upper surface of the trackbed to account for the weight of the rail tracks and sleepers. As a result of the simulation, a total of 32,096 spheres were used for the trackbed, inclusive of 12,758 spheres for the geocell panel, and 19,338 spheres (equally 1,612 clumps) for the ballast. In the case of control trackbed simulation, it involved similar quantities of spheres (20,248) or clumps (1,687) for the ballast infill, but saved spheres for the geocell panel.

Two loading scenarios were assessed: static and cyclic. Similar to plate loading tests developed for soil layers or piling foundations, the static loading aims to determine the ultimate bearing capacity of the ballast trackbed, as well as elastoplastic subsidence due to constant loading. The static loading scenario was achieved by compressing the complete upper surface of the trackbed using a wall. The wall was configured to move downwards at a constant rate of 0.1 mm/s until an axial strain of 20% was achieved. The limiting value of 20% is consistent with those set for calibration purposes, and reflects extreme subsidence occurring in practice. Cyclic loading is of further importance in regard to the assessment of the trackbed. The trackbed is designed to be subjected to cyclic impact of passing trains. Cyclic impact causes trackbed subsidence due to the cumulative plastic deformation (such as ballast rearrangement and track shoulder movement), which compromises serviceability of the trackbed. To assess these, a load of 294 kPa was applied to the wall through loading-unloading-reloading cycle. The load of 294 kPa was designed to be higher than the standard pressure generated by a train wagon travelling at a speed of 60 km/h (ARTC 2011). This was trialled in order to amplify the loading conditions and expedite the simulation process. In this study, a total of 50 cycle were accomplished as a preliminary assessment of the motion of the ballast. Implementation of additional cycle is achievable depending upon research needs and computational efficiency.

3. RESULTS AND DISCUSSION

Figure 6 presents simulation results of trackbed subsidence under both static and cyclic loading scenarios. Figure 6(a) shows the curves of vertical load vs. vertical strain for trackbeds subjected to static loading. Two trackbeds are examined: unreinforced (control) and geocell-reinforced. Comparison between the curves is facilitated when the loading curves are divided into three zones: *A*, *B* and *C*. Zone *A*, within a vertical load of 150 kPa, involves a linear relationship for both trackbeds. In this zone, both trackbeds settle to a similar extent and exhibit identical gradients, i.e. equal stiffness of

the trackbeds. This implies that the skeleton of the ballast bears the majority of the static load when the trackbed is subjected to a relatively low load or in the early stages of displacement-controlled loading. In zone *A*, the subsidence strain is up to 4%.

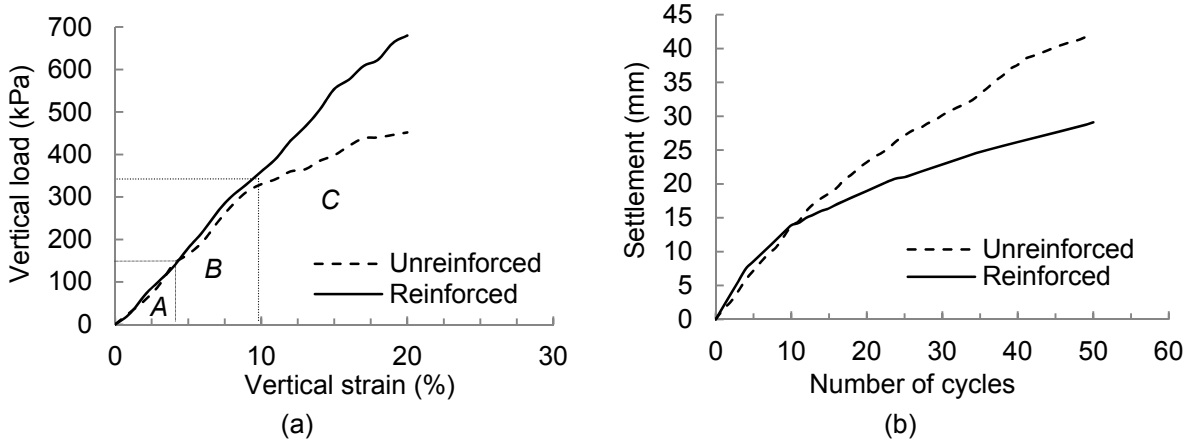

Figure 6. Simulation results of trackbed subsidence: (a) static loading, and (b) cyclic loading

Zone *B* involves the range of loading from 150 to 340 kPa, and a vertical strain of up to 9.7%. This range of load covers the working load of a train wagon and is acknowledged as a critical section in the assessment of trackbed performance. In this zone, the curve for the unreinforced trackbed starts to deviate from the linear trendline observed in Zone *A*, whereas the geocell-reinforced trackbed maintains this linear trendline, i.e. with a constant stiffness of the trackbed. The constant stiffness is expected to be associated with load-enhancing capability of the embedded geocell panel. Zone *C* is defined as the 'high loading' zone, which helps gain an understanding of the trackbed performance under extreme loading conditions. The improvement resulted from using geocell is particularly evident in this zone. For instance, at the same axial strain, the corresponding applied stress on the reinforced embankment is much higher than that of the unreinforced case, which implies the geocell-reinforced model can withstand much higher load. In addition, with the unreinforced trackbed, the stiffness continues to decrease and eventually levels off. For the reinforced trackbed, on the other hand, the stiffness remains largely constant until the limiting strain is achieved. This further confirms the load-enhancing capability of the geocell panel under high loading conditions.

Figure 6(b) shows the curves of settlement vs. number of cycles for the reinforced and unreinforced trackbeds subjected to cyclic loading. There is no discernible discrepancy between the two curves until the 11^{th} cycle takes place when a settlement of 13 mm occurs in both trackbeds. From the 12^{th} cycle onwards, the efficacy of the geocell to minimise settlement is observed. The curve for the geocell-reinforced trackbed exhibits a much smaller settlement rate than the unreinforced trackbed. As a result, the settlements differ significantly at the end of 50 cycles; 29 mm for the reinforced trackbed and 42 mm for the unreinforced trackbed, which amounts to a 30% reduction in trackbed subsidence owning to the embedment of geocell panel in ballast trackbed.

In addition to the above macro-mechanical response of the trackbeds, micro-mechanical characteristics of the ballast and geocell panel are observed from the front of the embankment, in Figure 7, which shows the distribution of contact forces for the unreinforced and reinforced trackbeds, respectively, under cyclic loading. It is observed that the contact forces develop in different patterns within the two trackbeds. The unreinforced trackbed has an uneven distribution of contact forces. The forces at the base of the trackbed are higher (a darker strip) than elsewhere in the trackbed. In contrast, the contact forces for the geocell-reinforced trackbed are more evenly distributed. Such an even distribution of contact forces is preferable in order to reduce the likelihood of localised failure, and thus improve the resilience of the trackbed.

Figure 8 shows perspectives of displacement vectors indicative of the motion of the particles. It can be seen that the lateral movement is less significant for the reinforced trackbed [Figure 8(a)] than for the unreinforced trackbed [Figure 8(b)]. In addition, the strip of ballast reinforced by the geocell panel [at the base of Figure 8(b)] show more active displacement in relation to the particles in the same location as those in the unreinforced trackbed. That is, the lateral ballast movement is partially offset by the motion of the particles restricted within the geocell strip. This is consistent with the distribution of

contact forces shown in Figure 7, which suggests that the higher the contact forces, the more likely the particles are prone to displace outward. The motion of the ballast confined within the geocell panel is reflected by the displacement vectors of the geocell spheres, as shown in Figure 8(c). It can be seen that the geocell undergoes deformation and, in some locations, translation. This relatively modest movement of the geocell helps to accommodate the motion of the ballast and reduce some of the ballast contact forces, while confining the ballast largely in its original location.

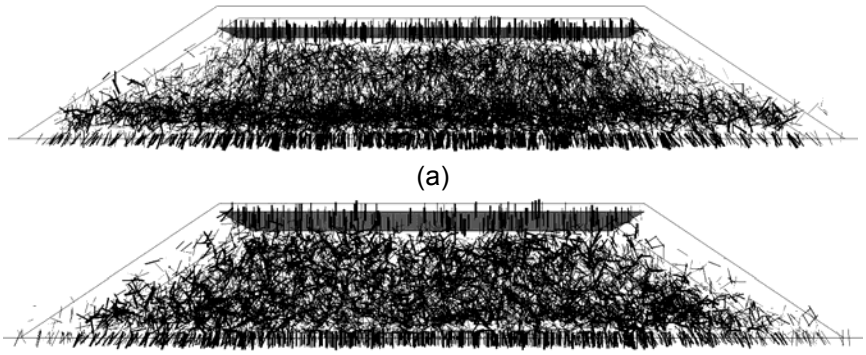

(a)

(b)

Figure 7. Perspectives of contact forces after the 20th cycle : (a) unreinforced, and (b) reinforced

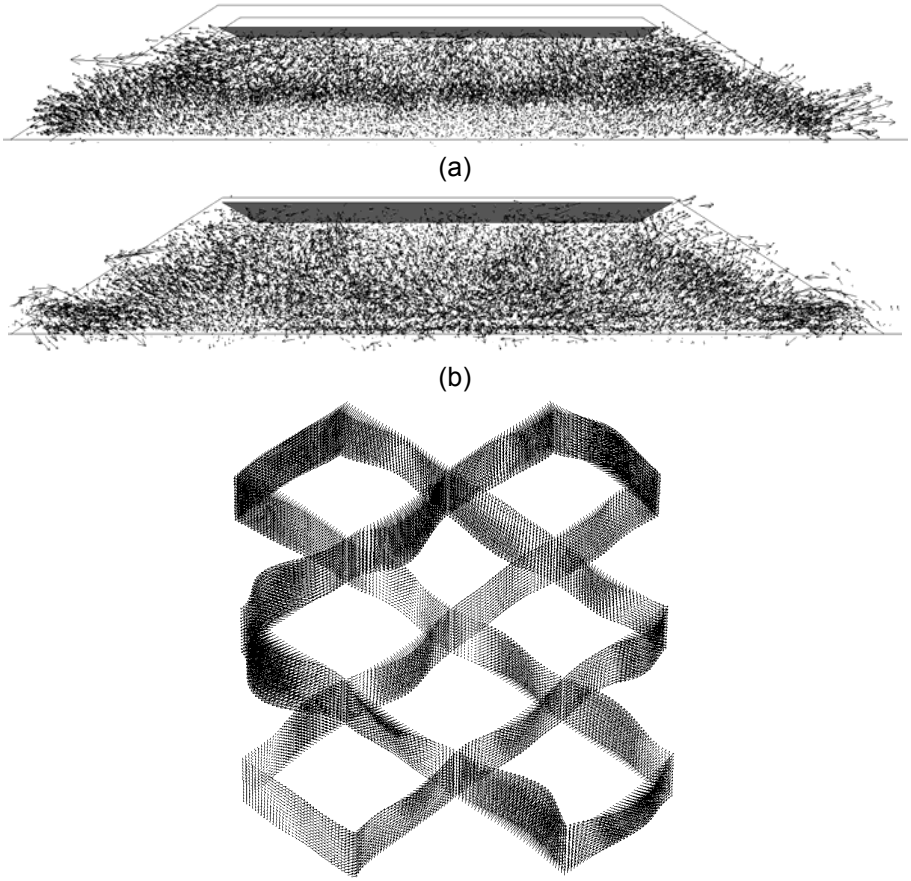

(a)

(b)

(c)

Figure 8. Perspectives of displacement vectors of spheres after the 20th cycle: (a) unreinforced (ballast spheres), (b) reinforced (ballast spheres), and (c) reinforced (geocell spheres)

4. CONCLUSION

This study has assessed the performance of a geocell-reinforced ballast trackbed. To achieve this, discrete element modelling was conducted to assess the mechanical response of the trackbed under static and cyclic loading conditions. Sphere clumps were developed to mimic real track ballast. Input

parameters for all spheres involved in the simulation were calibrated against laboratory test results. Modelling showed that embedment of geocell into the trackbed enhances stiffness of the trackbed under the static loading. The reinforced trackbed exhibited reduced subsidence and lateral displacement when compared with the unreinforced trackbed. This rises from the capacity of the geocell panel to reduce the motion of the ballast, offset localised contact forces and more evenly distribute the movement of the entire trackbed. The results of this preliminary study suggest that the incorporation of geocell reinforcement in rail trackbeds provides great potential for reducing their capital and maintenance costs.

5. ACKNOWLEDGEMENTS

This study was conducted with the support of Geofabrics SA who donated a standard geocell panel and shared technical specifications of the panel, and is highly appreciated.

REFERENCES

ARTC (2006). “Engineering practices manual – Civil Engineering.” Australian Rail Track Corporation, Adelaide SA, Australia.

Chen, C., McDowell, G. R., and Thom, N. H. (2012). “Discrete element modelling of cyclic loads of geogrid-reinforced ballast under confined and unconfined conditions.” Geotextiles and Geomembranes, 35, 76-86.

Dash, S.K. (2012). “Effect of geocell type on load-carrying mechanisms of geocell–reinforced sand foundations.” International Journal of Geomechanics, 12 (5), 537-548.

Indraratna, B., Ionewscu, D., and Christie, H. D. (1998). “Shear behavior of railway ballast based on large-scale triaxial tests.” Journal of Geotechnical and Geoenvironmental Engineering, 124 (5), 439-449.

Indraratna, B., Nimbalkar, S., Christie, D., Rujikiatkamjorn, C., and Vinod, J. (2010). “Field assessment of the performance of a ballasted rail track with and without geosynthetics.” Journal of Geotechnical and Geoenvironmental Engineering, 136 (7), 907-917.

ITASCA (2008). PFC3D 4.0 User Manual. Itasca Consulting Group, Inc., Minneapolis, MN 55401, USA.

Le Pen, L. M., Powrie, W., Zervos, A., Ahmed, S., and Aingaran, S. (2013). “Dependence of shape on particle size for a crushed rock railway ballast.” Granular Matter, 15 (6), 849-861.

Leshchinsky, B., and Ling, H.I. (2013). “Numerical modeling of behavior of railway ballasted structure with geocell confinement.” Geotextiles and Geomembranes, 36, 33-43.

Lu, M., and McDowell, G. R. (2006). “The importance of modelling ballast particle shape in the discrete element method.” Granular Matter, 9 (1-2), 69-80.

Potyondy, D. O., and Cundall, P. A. 2004. “A bonded-particle model for rock. International Journal of Rock Mechanics and Mining Sciences, 41, 1329-1364.

Yang, X.M. (2010). “Numerical analyses of geocell reinforced granular soils under static and repeated loads.” A PhD thesis, The University of Kansas, 193 p.